







## Doubly differential cross sections for ionization in proton collisions with atomic hydrogen: Energy and angular distribution of emitted electrons

C. T. Plowman <sup>1,\*</sup>, K. H. Spicer <sup>1</sup>, N. W. Antonio <sup>1</sup>, M. S. Schöffler <sup>2</sup>, M. Schulz,<sup>3</sup> I. Bray <sup>1</sup> and A. S. Kadyrov <sup>1,4</sup>

<sup>1</sup>*Department of Physics and Astronomy, Curtin University, GPO Box U1987, Perth WA 6845, Australia*

<sup>2</sup>*Institut für Kernphysik, Universität Frankfurt, 60438 Frankfurt, Germany*

<sup>3</sup>*Physics Department and LAMOR, Missouri University of Science and Technology, Rolla, Missouri 65409, USA*

<sup>4</sup>*Institute of Nuclear Physics, Ulugbek, Tashkent 100214, Uzbekistan*



(Received 10 May 2024; revised 1 July 2024; accepted 9 July 2024; published 6 August 2024)

We use the two-center wave-packet convergent close-coupling approach to ion-atom collisions to calculate the energy and angular distribution of electrons emitted in proton collisions with atomic hydrogen. Results are provided across a wide range of intermediate energies where many competing reaction channels make calculations challenging. The present data consistently agree with the available experimental measurements and improve upon previously available results based on perturbative and classical methods. Furthermore, we extend the range of electron angles and energies over which theoretical data are available for the doubly differential cross section for ionization. This provides strong evidence that at the level of doubly differential cross sections nonperturbative high-order methods are required to accurately model the ionization process.

DOI: [10.1103/PhysRevA.110.022804](https://doi.org/10.1103/PhysRevA.110.022804)

### I. INTRODUCTION

Ion-atom collisions underpin a number of state-of-the-art technologies such as nuclear-fusion energy [1] and hadron therapy of cancer [2]. Coupled with the fundamental significance of these processes this has resulted in a continuing interest in studying collisions of many different ion species with various targets [3,4]. The ionization process has received particular attention recently [5,6] thanks to the development of advanced experimental techniques like cold target recoil ion momentum spectroscopy [7]. This method has allowed kinematically complete experiments capable of measuring the fully differential cross section (FDCS) for ionization [8–10].

The proton-hydrogen collision system represents the simplest system for which the Schrödinger equation is not analytically solvable. It has therefore provided a testing ground for scattering theories ranging from the early studies of electron capture using the first-order Born approximation (FBA) [11–14] to the development of more sophisticated methods such as the continuum-distorted-wave (CDW) approach [15–18] and close-coupling formalism [19–26]. With only a single electron, there are no exchange effects. The interaction potentials and target wave functions are analytically known. However, experimental measurements for  $p + \text{H}$  collisions are significantly less common than for other more complex target species such as He and  $\text{H}_2$ . This can be attributed mainly to the difficulties in preparing an atomic hydrogen target [27]. The majority of experimental data on  $p + \text{H}$  collisions is for integrated cross sections such as the total electron-capture cross section (see, e.g., Refs. [28–31]) and the total ionization cross section (TICS) (see, e.g.,

Refs. [32,33]). Only after the measurements by Kerby III *et al.* [27] was a comprehensive experimental investigation of the differential cross sections for ionization performed for  $p + \text{H}$  collisions. They measured the doubly differential cross section (DDCS) for ionization, as a function of the energy and angle of the emitted electron. This is a significantly more detailed quantity than the integrated cross section for ionization and exhibits a number of interesting features resulting from various physical mechanisms. A striking feature is the electron capture into the continuum (ECC) peak which occurs at an electron velocity,  $v_e$ , matching that of the projectile,  $v_i$  [34]. It also results in an enhancement of the DDCS when electrons are emitted in the forward direction. In another mechanism the projectile collides directly with the target electron, transferring momentum such that the electron is emitted with twice the speed of the projectile [35]. This is known as the binary-encounter mechanism and results in a broad peak centered near  $v_e = 2v_i$  for emission in the forward direction.

Kerby III *et al.* [27] applied a number of commonly used theoretical methods to assess their range of applicability by comparison to the measured DDCS for ionization. Namely, these were the FBA, the continuum-distorted-wave eikonal-initial-state (CDW-EIS) approach, and the classical trajectory Monte Carlo (CTMC) method. The first two of these are based on the assumption that the changes to the electronic wave function can be modeled as small perturbations. This idea is only applicable when the speed of the incident proton is substantially larger than the classical orbital speed of the electron. Contrastingly, the CTMC approach is based on solving the classical equations of motion for a large ensemble of trajectories and recovering information about the outcome of scattering from statistical analysis. Calculations were performed at five collision energies, from 20 to 114 keV. As expected, the FBA and CDW-EIS approaches failed to accu-

\*Contact author: [corey.plowman@curtin.edu.au](mailto:corey.plowman@curtin.edu.au)

rately model the energy and angular distribution of emitted electrons at the lower impact energies. Improved agreement was found for faster collisions, although the FBA significantly overestimated the number of low-energy electrons emitted at backward angles (angles larger than  $90^\circ$ ). Meanwhile, the CDW-EIS results were in better agreement with the experiment but for large emission angles tended to underestimate the measurements. The CTMC calculations were also reasonably in agreement with the data, but they significantly overestimated or underestimated the DDCS for ionization at some energies and angles. Overall, agreement between existing theory and the experiment for the DDCS measured by Kerby III *et al.* [27] is mixed at best, with the greatest differences observed at the smallest experimentally considered collision energy of 20 keV.

Other perturbative calculations of the DDCS for ionization differential in the energy and angle of the emitted electron include the continuum-correlated wave eikonal-initial-state (CCW-EIS1) approach [36] and the method based on the Coulomb-distorted three-body plane wave [37]. In the standard CDW-EIS approach, the final-state wave function is written as the product of the two-body Coulomb wave for the electron-target and electron-projectile systems. Colavecchia *et al.* [36] instead expanded the final-state wave function in terms of both target- and projectile-centered two-body Coulomb functions. They also used this correlated wave function in the FBA, labeling this as the Born- $\Phi_2$  model. The CCW-EIS1 results were very similar to the CDW-EIS calculations by Kerby III *et al.* [27] at 114 keV, except for high-energy electrons where the former was found to underestimate the experimental data whereas the latter followed the measurements more closely. The Born- $\Phi_2$  approach was in much better agreement with experiment in some kinematic regions compared to the FBA calculations. The approach of Berakdar [37] is similar. They calculated the DDCS at 95 keV. For  $15^\circ$  emission, the results underestimated the experiment up to 200 eV, then overestimated the cross section for high-energy electrons. Unexpectedly, agreement was substantially better for electrons emitted at  $150^\circ$ .

Accurately calculating the DDCS for ionization is an essential step towards applying theory to the most detailed quantity describing the ionization process: the FDCS. To date, the FDCS for ionization in collisions of protons with atoms and molecules at intermediate energies has only been studied with perturbative methods. Significant discrepancies remain between theory and experiment [8,38]. The CDW-EIS approach was first applied to calculate the FDCS for ionization in  $p + H$  collisions by Jones and Madison [39]. However, as there are no experimental measurements of the FDCS for the atomic hydrogen target, it was impossible to judge the accuracy of the results. Subsequent investigations focused on proton collisions with  $H_2$  [9,40] and He [5,38]. Quantitative and qualitative differences between the measurements and calculations were observed, highlighting the need for more advanced methods that can account for the coupling effects between the reaction channels to be applied to the problem.

In this paper we apply the wave-packet convergent close-coupling (WP-CCC) approach to resolve the outstanding disagreement between theory and experiment regarding the energy and angular distribution of electrons emitted in

intermediate-energy  $p + H$  collisions. We restrict ourselves to collisions where the target is initially in the ground ( $1s$ ) state. In this energy region, there are many competing reaction channels that must be accounted for on an equal footing. Of particular importance is the possibility of capture of the electron by the projectile resulting in the formation of a fast-traveling, possibly excited, atom and ionization which results in three free particles in the final channel. Both of these mechanisms, as well as elastic scattering and target excitation, play important roles in the collisional dynamics, making accurate modeling difficult. Close-coupling methods are capable of accounting for the interaction between all reaction channels throughout the collision. Historically, two major drawbacks have restricted the utility of the close-coupling approaches when applied to ion-atom collisions. First, the robustness of the results is ascertained only by assessing the convergence with an increase in the number of basis states used to expand the total scattering wave function. However, as the basis size is increased the computational requirements become increasingly demanding. Second, the non- $L^2$  nature of the Coulomb wave function results in unbounded integrals in the scattering equations, preventing straightforward inclusion of the electron continuum and, consequently, modeling of the ionization process. The WP-CCC approach [41,42] has been developed to address these obstacles and accounts for the continuum through the use of stationary wave-packet pseudostates and the surface-integral formulation of scattering theory [43] to determine the ionization amplitudes. Furthermore, it makes use of highly efficient GPU-enabled codes that allow for very large calculations with many thousands of basis states [44]. The WP-CCC approach has been successfully applied to the calculation of various types of differential cross sections for ionization in  $p + H$  [42,45],  $p + He$  [46–48],  $p + H_2$  [49–52], and  $He^{2+} + He$  [53,54] collisions. Here we consider the DDCS differential in the energy and ejection angle of the electron for  $p + H$  collisions. Unless specified otherwise, atomic units (a.u.) are used throughout this paper.

## II. WAVE-PACKET CONVERGENT CLOSE-COUPPING METHOD

The two-center WPCCC approach is described in detail in Refs. [41,42]. Here we describe the essential parts that relate to the present paper. The approach begins with the full three-body Schrödinger equation which has a parametric dependence on time through the internuclear distance  $R$ :

$$(H - E)\Psi_i^+ = 0. \quad (1)$$

Here  $H$  is the full Hamiltonian of the collision system,  $E$  is the total energy, and  $\Psi_i^+$  is the total scattering wave function subject to the outgoing-wave boundary conditions. The latter is expanded in terms of  $N^T$  target-centered pseudostates,  $\psi_\alpha^T$ , and  $N^P$  projectile-centered pseudostates,  $\psi_\beta^P$ , according to

$$\begin{aligned} \Psi_i^+ \approx & \sum_{\alpha=1}^{N^T} F_\alpha(\sigma_T) \psi_\alpha^T(\mathbf{r}_T) e^{iq_\alpha \cdot \sigma_T} \\ & + \sum_{\beta=1}^{N^P} G_\beta(\sigma_P) \psi_\beta^P(\mathbf{r}_P) e^{iq_\beta \cdot \sigma_P}, \end{aligned} \quad (2)$$

where  $F_\alpha$  and  $G_\beta$  are unknown expansion coefficients,  $\mathbf{r}_T$  ( $\mathbf{r}_P$ ) is the position of the electron relative to the target (projectile) nucleus,  $\mathbf{q}_\alpha$  ( $\mathbf{q}_\beta$ ) is the momentum of the projectile ion (atom) relative to the target atom (residual ion), and  $\boldsymbol{\sigma}_T$  ( $\boldsymbol{\sigma}_P$ ) is the Jacobi coordinate of the projectile ion (atom) relative to the target atom (residual ion). The basis functions are constructed from eigenstates of the hydrogen atom for negative energies and wave packets formed by integrating the Coulomb wave over discrete momentum bins for positive energies. This allows us to describe both binary and breakup processes (including coupling between the bound and continuum spectra) all while using a square-integrable basis. For the collision energies considered herein (20 keV and above), the semiclassical impact-parameter approximation can be applied. The projectile ion is assumed to follow a classical trajectory parametrized by time  $t$  with position  $\mathbf{R}(t) = \mathbf{b} + \mathbf{v}_i t$  relative to the target nucleus, where  $\mathbf{b}$  is the impact parameter, set perpendicular to  $\mathbf{v}_i$ , the initial velocity of the projectile. This relative motion is represented by the plane waves in the expansion (2). Furthermore, the semiclassical approximation allows us to write  $F(\boldsymbol{\sigma}_T) \approx F(t, \mathbf{b})$  and  $G(\boldsymbol{\sigma}_P) \approx G(t, \mathbf{b})$ , effectively introducing a time dependence to the expansion coefficients. Substituting this expansion into the exact Schrödinger equation and applying the semiclassical approximation leads to the following set of first-order differential equations [55]:

$$\begin{aligned} i\dot{F}_{\alpha'} + i \sum_{\beta=1}^{N^P} \dot{G}_\beta K_{\alpha'\beta}^T &= \sum_{\alpha=1}^{N^T} F_\alpha D_{\alpha'\alpha}^T + \sum_{\beta=1}^{N^P} G_\beta Q_{\alpha'\beta}^T, \\ i \sum_{\alpha=1}^{N^T} \dot{F}_\alpha K_{\beta'\alpha}^P + i\dot{G}_{\beta'} &= \sum_{\alpha=1}^{N^T} F_\alpha Q_{\beta'\alpha}^P + \sum_{\beta=1}^{N^P} G_\beta D_{\beta'\beta}^P, \\ \alpha' &= 1, 2, \dots, N^T, \\ \beta' &= 1, 2, \dots, N^P. \end{aligned} \quad (3)$$

Here, dots over  $F_\alpha$  and  $G_\beta$  denote derivatives with respect to  $t$ . In Eq. (3) we omit the functional dependence of the matrix elements and expansion coefficients on  $\mathbf{R}$  for conciseness. The direct-scattering matrix elements are written as

$$\begin{aligned} D_{\alpha'\alpha}^T &= e^{i(\varepsilon_{\alpha'}^T - \varepsilon_\alpha^T)t} \langle \psi_{\alpha'}^T | \bar{V}_T | \psi_\alpha^T \rangle, \\ D_{\beta'\beta}^P &= e^{i(\varepsilon_{\beta'}^P - \varepsilon_\beta^P)t} \langle \psi_{\beta'}^P | \bar{V}_P | \psi_\beta^P \rangle, \end{aligned} \quad (4)$$

where

$$\begin{aligned} \bar{V}_T &= \frac{1}{R} - \frac{1}{|\mathbf{r}_T - \mathbf{R}|}, \\ \bar{V}_P &= \frac{1}{R} - \frac{1}{|\mathbf{r}_P - \mathbf{R}|}. \end{aligned} \quad (5)$$

The overlap integrals are

$$\begin{aligned} K_{\beta'\alpha}^P &= e^{i(\varepsilon_{\beta'}^P - \varepsilon_\alpha^T)t} e^{-i\mathbf{v}_i \cdot \mathbf{r}_P / 2} \langle \psi_{\beta'}^P | e^{-i\mathbf{v}_i \cdot \mathbf{r}_P} | \psi_\alpha^T \rangle, \\ K_{\alpha'\beta}^T &= e^{i(\varepsilon_{\alpha'}^T - \varepsilon_\beta^P)t} e^{-i\mathbf{v}_i \cdot \mathbf{r}_T / 2} \langle \psi_{\alpha'}^T | e^{i\mathbf{v}_i \cdot \mathbf{r}_T} | \psi_\beta^P \rangle, \end{aligned} \quad (6)$$

and the exchange matrix elements are

$$\begin{aligned} Q_{\beta'\alpha}^P &= e^{-i\mathbf{v}_i \cdot \mathbf{r}_T / 2 + i(\varepsilon_{\beta'}^P - \varepsilon_\alpha^T)t} \\ &\quad \times \langle \psi_{\beta'}^P | e^{-i\mathbf{v}_i \cdot \mathbf{r}_P} (H_T + \bar{V}_T - \varepsilon_\alpha^T) | \psi_\alpha^T \rangle, \\ Q_{\alpha'\beta}^T &= e^{-i\mathbf{v}_i \cdot \mathbf{r}_T / 2 + i(\varepsilon_{\alpha'}^T - \varepsilon_\beta^P)t} \\ &\quad \times \langle \psi_{\alpha'}^T | e^{i\mathbf{v}_i \cdot \mathbf{r}_T} (H_P + \bar{V}_P - \varepsilon_\beta^P) | \psi_\beta^P \rangle, \end{aligned} \quad (7)$$

where the target- and projectile-atom Hamiltonians are given by

$$\begin{aligned} H_T &= -\frac{1}{2} \nabla_{\mathbf{r}_T}^2 - \frac{1}{r_T}, \\ H_P &= -\frac{1}{2} \nabla_{\mathbf{r}_P}^2 - \frac{1}{r_P}, \end{aligned} \quad (8)$$

and  $\varepsilon_\alpha^T$  ( $\varepsilon_\beta^P$ ) is the energy of the target (projectile) state  $\alpha$  ( $\beta$ ).

Equation (3) is solved subject to the initial condition

$$\begin{aligned} F_\alpha(-\infty, \mathbf{b}) &= \delta_{\alpha 1}, \quad \alpha = 1, 2, \dots, N^T, \\ G_\beta(-\infty, \mathbf{b}) &= 0, \quad \beta = 1, 2, \dots, N^P. \end{aligned} \quad (9)$$

We set  $i = 1$  in Eq. (9) to represent the electron in the ground state of the target in the incident channel.

The differential cross section for ionization is determined from the expansion coefficients according to the method outlined in Ref. [51]. Briefly, we start with the general post form of the on-shell  $T$  matrix [56]:

$$T_{fi}(\mathbf{q}_f, \mathbf{q}_i) = \langle \Phi_f^- | \overleftarrow{H} - E | \Psi_i^+ \rangle, \quad (10)$$

where  $\mathbf{q}_f$  and  $\mathbf{q}_i$  are the relative momenta in the final and initial channels, respectively, and  $\Phi_f^-$  is the asymptotic state corresponding to the final channel. The arrow over the Hamiltonian indicates the direction of action. We then insert the identity operator constructed from our target- and projectile-centered square-integrable pseudostates. This splits the amplitude into two parts, direct ionisation (DI) and ECC. In the first part, the action of the identity operator constructed from the target-centered pseudostates leads to limiting the target subspace by replacing the full set of the target states (including non- $L^2$  continuum) with a set of  $L^2$  pseudostates. This effectively screens the interaction between the projectile and target constituents, even in the continuum. Likewise, the action of the operator constructed from the projectile-centered pseudostates limits the projectile subspace by replacing the full set of projectile states (including non- $L^2$  continuum) with a set of  $L^2$  pseudostates.

The DI amplitude is written as

$$T_{fi}^{\text{DI}}(\boldsymbol{\kappa}, \mathbf{q}_f, \mathbf{q}_i) = \sum_{\ell_\alpha m_\alpha} \langle \psi_\kappa^T | \psi_\alpha^T \rangle T_{fi}^{\text{DS}}(\mathbf{q}_f, \mathbf{q}_i), \quad (11)$$

and in the case of electron capture into the continuum of the projectile we write the amplitude as

$$T_{fi}^{\text{ECC}}(\boldsymbol{\kappa}, \mathbf{q}_f, \mathbf{q}_i) = \sum_{\ell_\beta m_\beta} \langle \psi_\kappa^P | \psi_\beta^P \rangle T_{fi}^{\text{EC}}(\mathbf{q}_f, \mathbf{q}_i). \quad (12)$$

The  $T$ -matrix elements for direct scattering (DS),  $T_{fi}^{\text{DS}}$ , and electron capture (EC),  $T_{fi}^{\text{EC}}$ , are calculated from the expansion coefficients using the Fourier transform. The overlap between the Coulomb wave and our wave-packet pseudostates can be

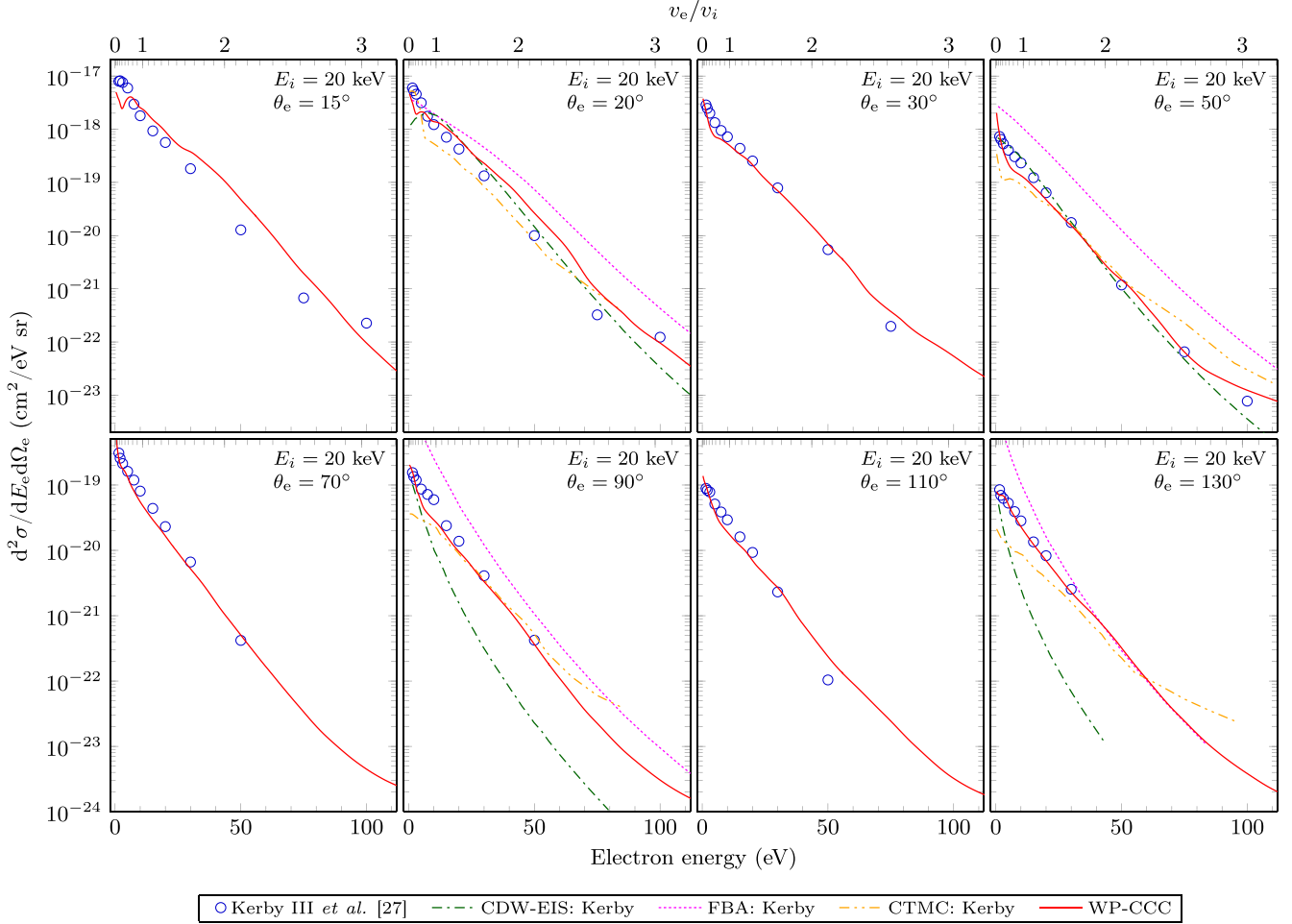


FIG. 1. Doubly differential cross sections for ionization in 20-keV  $p + \text{H}$  collisions as functions of the electron energy at various emission angles. Experimental data are by Kerby III *et al.* [27]. Theoretical results are the present WP-CCC approach, FBA, CDW-EIS approach, and CTMC approach by Kerby III *et al.* [27].

calculated analytically and is given in Ref. [51] for a one-electron system. Finally, the FDCS for ionization resulting in an electron with energy  $E_e$  emitted into the solid angle  $\Omega_e$  and the projectile being scattered into  $\Omega_f$  is

$$\frac{d^3\sigma}{dE_e d\Omega_e d\Omega_f} = \frac{\mu_T^2}{(2\pi)^5} \frac{\kappa q_f}{q_i} \left[ |T_{fi}^{\text{DI}}(\boldsymbol{\kappa}, \mathbf{q}_i, \mathbf{q}_f)|^2 + |T_{fi}^{\text{ECC}}(\boldsymbol{\kappa} - \mathbf{v}, \mathbf{q}_i, \mathbf{q}_f)|^2 \right], \quad (13)$$

where  $\mu_T$  is the reduced mass of the projectile-ion and target-atom system. Before combining, the ECC component must be transformed into a common frame of reference with the DI part. We choose the laboratory frame as a common coordinate system. Therefore, the DI amplitude given by Eq. (11) does not need to be transformed since it is defined in the laboratory frame. However, the ECC amplitude given by Eq. (12) is defined in the projectile frame and must, therefore, be converted. To do this, we substitute  $\boldsymbol{\kappa} - \mathbf{v}$  for  $\boldsymbol{\kappa}$  and  $(\mathbf{q}_p - \boldsymbol{\kappa})^\perp$  for the perpendicular momentum transfer,  $\mathbf{q}_p^\perp$ , in Eq. (12) to obtain (after integration) the amplitudes for charge transfer into the projectile continuum with electron momentum  $\boldsymbol{\kappa}$ .

Following the work of Refs. [42,51] we add the DI and ECC components incoherently in Eq. (13).

Comparison between the coherent and incoherent combination has shown [42] that the difference in the differential cross section is negligible. Furthermore, the results are calculated in the asymptotic state where the target and projectile square-integrable pseudostates do not overlap. Therefore, there should be little if any interference between these terms in the final channel in our approach [51].

The DDCS is obtained by integrating the FDCS in Eq. (13) over  $\Omega_f$ . This can be done analytically or numerically. Therefore, we have two methods to calculate the DDCS as a function of the energy and angle of the electron. We compared results from both approaches as a self-consistency check and found no appreciable difference in the cross section.

### III. COMPUTATIONAL IMPLEMENTATION

Full details of the computational implementation are given in Ref. [57]. To summarize, we use the fourth-order Runge-Kutta approach to compute the solution to the differential equations (3). The position of the projectile along the direction of incidence is discretized into 1500 steps ranging from  $z_{\min} = -300$  to  $z_{\max} = 300$  a.u. The points are distributed exponentially in a symmetric manner about  $z = 0$  such that

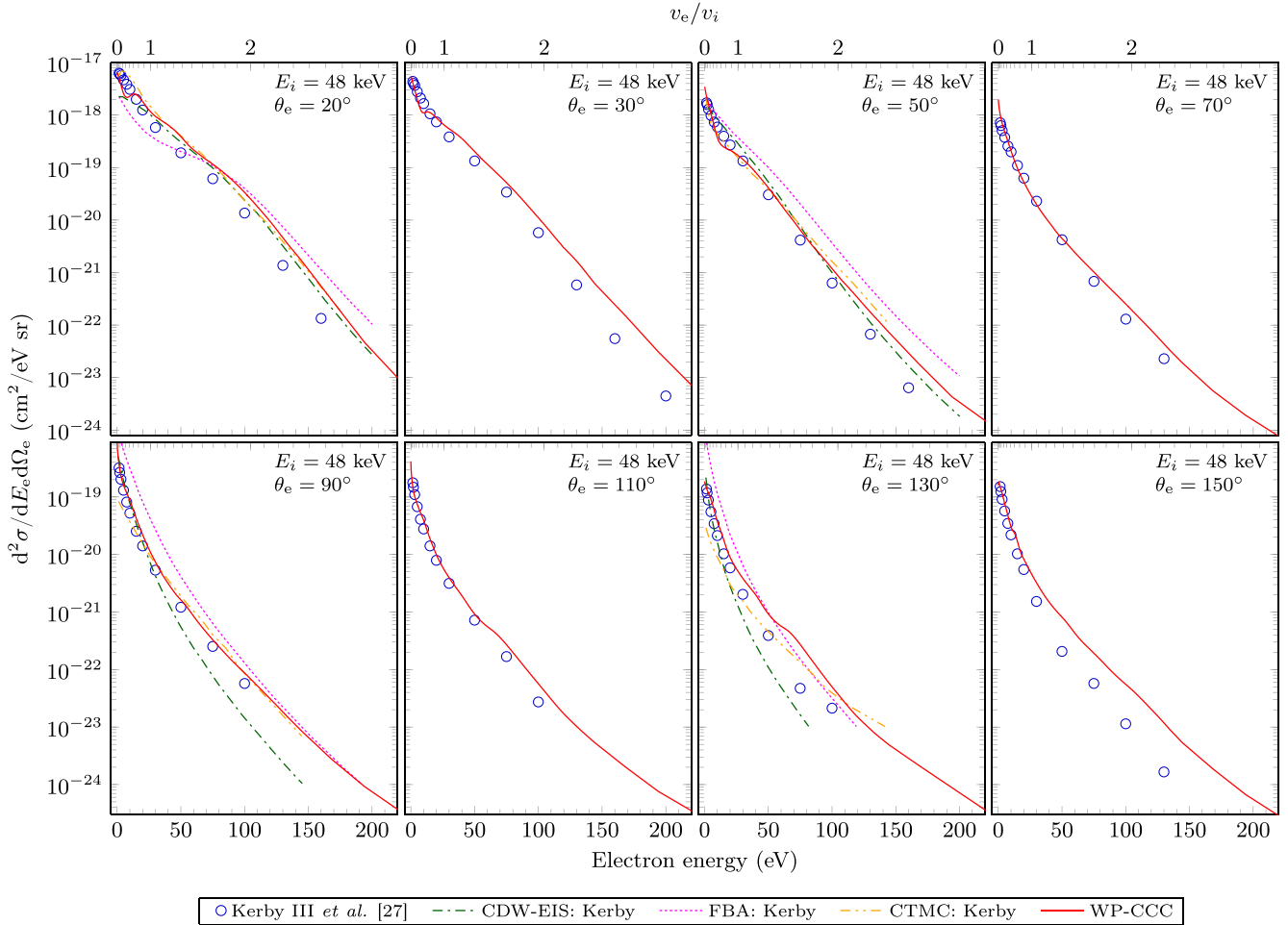


FIG. 2. Doubly differential cross sections for ionization in 48-keV  $p + \text{H}$  collisions as functions of the electron energy at various emission angles. Experimental data are by Kerby III *et al.* [27]. Theoretical results are the present WP-CCC approach, FBA, CDW-EIS approach, and CTMC approach by Kerby III *et al.* [27].

the density is highest near the scattering center. Equation (3) is solved at 64 different impact-parameter points ranging from 0 to 40 a.u. to ensure the probability for all reaction channels falls off by several orders of magnitude relative to the peak at small values of  $b$ .

The matrix elements given in Eqs. (4), (6), and (7) are evaluated using the method described in Ref. [42]. Briefly, the Coulomb interaction in Eq. (4) is expanded in partial waves allowing us to separate the radial and angular components of the integrals. Then, the integral over  $\hat{r}_T$  ( $\hat{r}_P$ ) can be taken analytically, leaving only the radial part to be computed numerically. Equations (6) and (7) are evaluated using prolate spheroidal coordinates in the rotating molecular frame where the elliptical coordinate foci are situated at the target and projectile nuclei. This allows us to write the integrals in terms of the spheroidal coordinates which are then numerically evaluated using Gauss-Legendre and Gauss-Laguerre quadratures. The number of integration points for both quadratures was increased until the results converged. We found that 200 points at 20 keV and 300 at the other energies was sufficient.

The radial integrals appearing in the direct-scattering matrix elements are evaluated using a Simpson rule quadrature with 5892 points that reduce in density towards  $r_{\text{max}} = 500$

a.u., where the basis functions become very small. Once again this was verified as sufficient by systematically increasing the size and density until convergence was obtained in the results.

It is important to note that the pseudostates used in expansion (2) are overcomplete. While the target-centered basis functions are mutually orthogonal and so are the projectile-centered basis functions, each set is not orthogonal to the other. In principle, this may introduce ill conditioning in the set of equations (3). To manage this we calculate the norm of the total-scattering wave function at every step in the  $z$  grid and check that it is equal to unity. This conservation of norm ensures that the results are not negatively affected by the use of nonorthogonal basis functions in the expansion.

#### IV. RESULTS

In this section we present our calculations of the doubly differential cross section,  $d^2\sigma/dE_e d\Omega_e$ , for ionization in  $p + \text{H}$  collisions as a function of the energy,  $E_e$ , of the electron ejected into the solid angle,  $\Omega_e$ . Results are shown for select emission angles,  $\theta_e$ , where experimental data are available. For all results presented here we use a symmetric basis, i.e., the same number of target- and projectile-centered states are

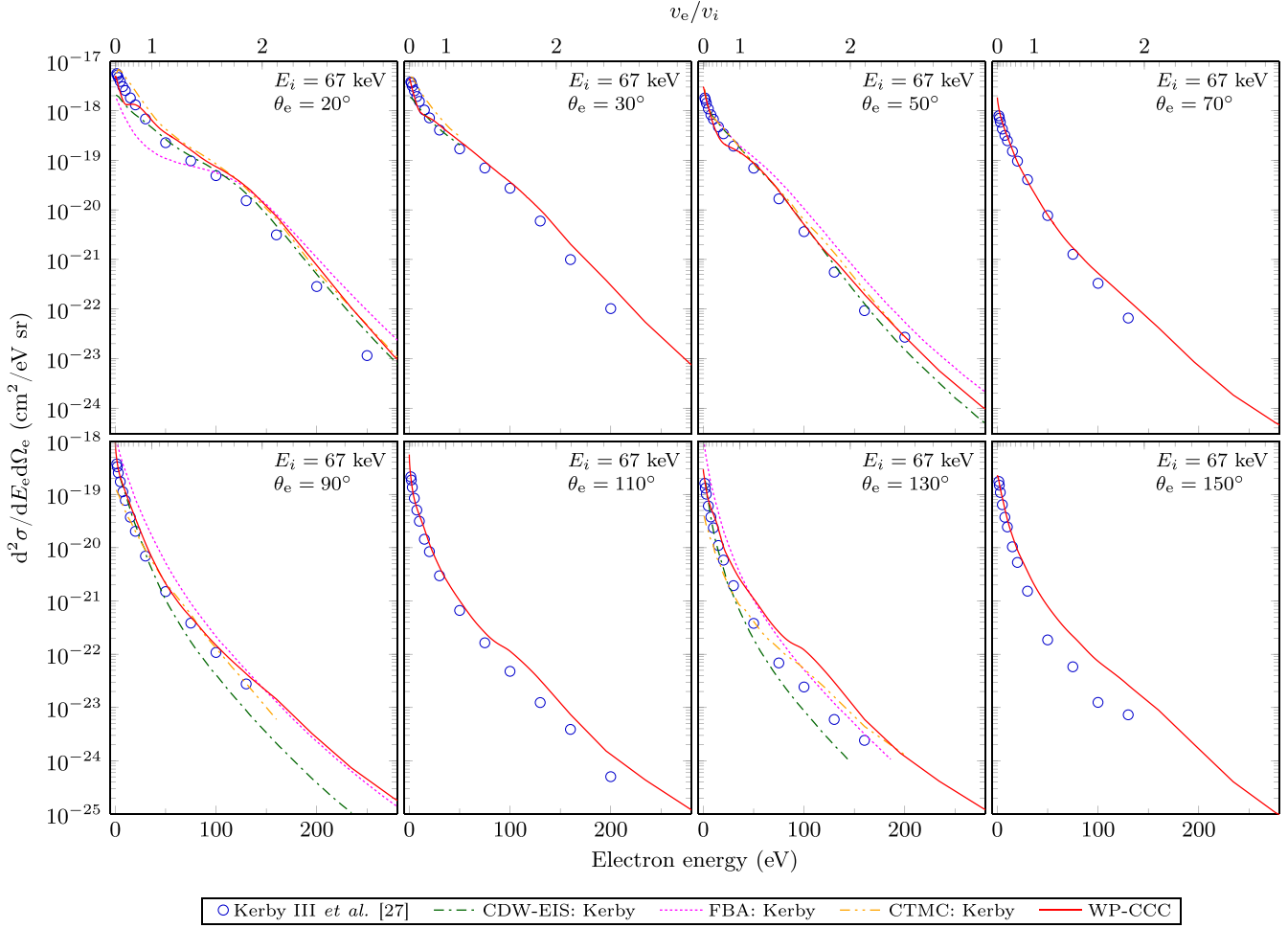


FIG. 3. Doubly differential cross sections for ionization in 67-keV  $p + \text{H}$  collisions as functions of the electron energy at various emission angles. Experimental data are by Kerby III *et al.* [27]. Theoretical results are the present WP-CCC approach, FBA, CDW-EIS approach, and CTMC approach by Kerby III *et al.* [27].

used in expansion (2). We find that a basis containing  $10 - \ell$  bound states for each orbital angular momentum up to a maximum of  $\ell_{\text{max}} = 5$  was sufficient to obtain convergence at 20 keV. At higher collision energies  $\ell_{\text{max}} = 3$  was found to be sufficient. The continuum was discretized with 25 bins and the maximum electron momentum varied from  $\kappa_{\text{max}} = 5$  to 10 a.u. depending on the collision energy. Numerical integration of the calculated DDCS over the entire energy and angular space of the electron reproduced the TICS within 1% of those calculated directly from the impact-parameter amplitudes reported in Ref. [58].

In Fig. 1, we present our results at the lowest considered energy of  $E_i = 20$  keV. Calculating differential cross sections for ionization at low energies is very challenging and we immediately see that the other calculations available in the literature fail to agree with the experimental measurements. Nevertheless, the WP-CCC results generally agree well with the experimental data by Kerby III *et al.* [27]. It is not surprising that perturbative approaches like the simple FBA and CDW-EIS do not work very well in this kinematic regime. The CTMC results are also generally in poor agreement with the measurements for 20 keV. In our results we observe a clear secondary peak, the electron capture into the continuum

(ECC) peak, near the energy corresponding to the electron having the same speed as the projectile. This is known as the matching speed and for 20-keV collisions is 0.894 a.u. The ECC peak is slightly shifted towards lower energies at  $15^\circ$ . A similar situation is observed at  $20^\circ$ , although to a lesser extent. This behavior is the same as observed for  $p + \text{He}$  collisions by Spicer *et al.* [59]. We note, however, that we do not see a shift of the peak position at  $0^\circ$  as reported in Refs. [60,61] for low-energy  $p + \text{He}$  and  $p + \text{H}_2$  collisions. For  $70^\circ$  (and  $110^\circ$ ) electron emission, the WP-CCC calculations are the only available theoretical results. Agreement with the measurements is quite good for both slow and fast electrons at this emission angle. The next panel shows ejection into the perpendicular plane. The WP-CCC result agrees well with the data here, providing improvement over the other theoretical results. The last two panels in Fig. 1 show data for electrons ejected into backward angles. We see that the present calculations are in good agreement with the experiment for  $110^\circ$  and  $130^\circ$ . At the largest angle considered the other three theoretical methods differ significantly from the measurements, leaving the WP-CCC results as the only method that is able to accurately describe the experiment at  $130^\circ$ .

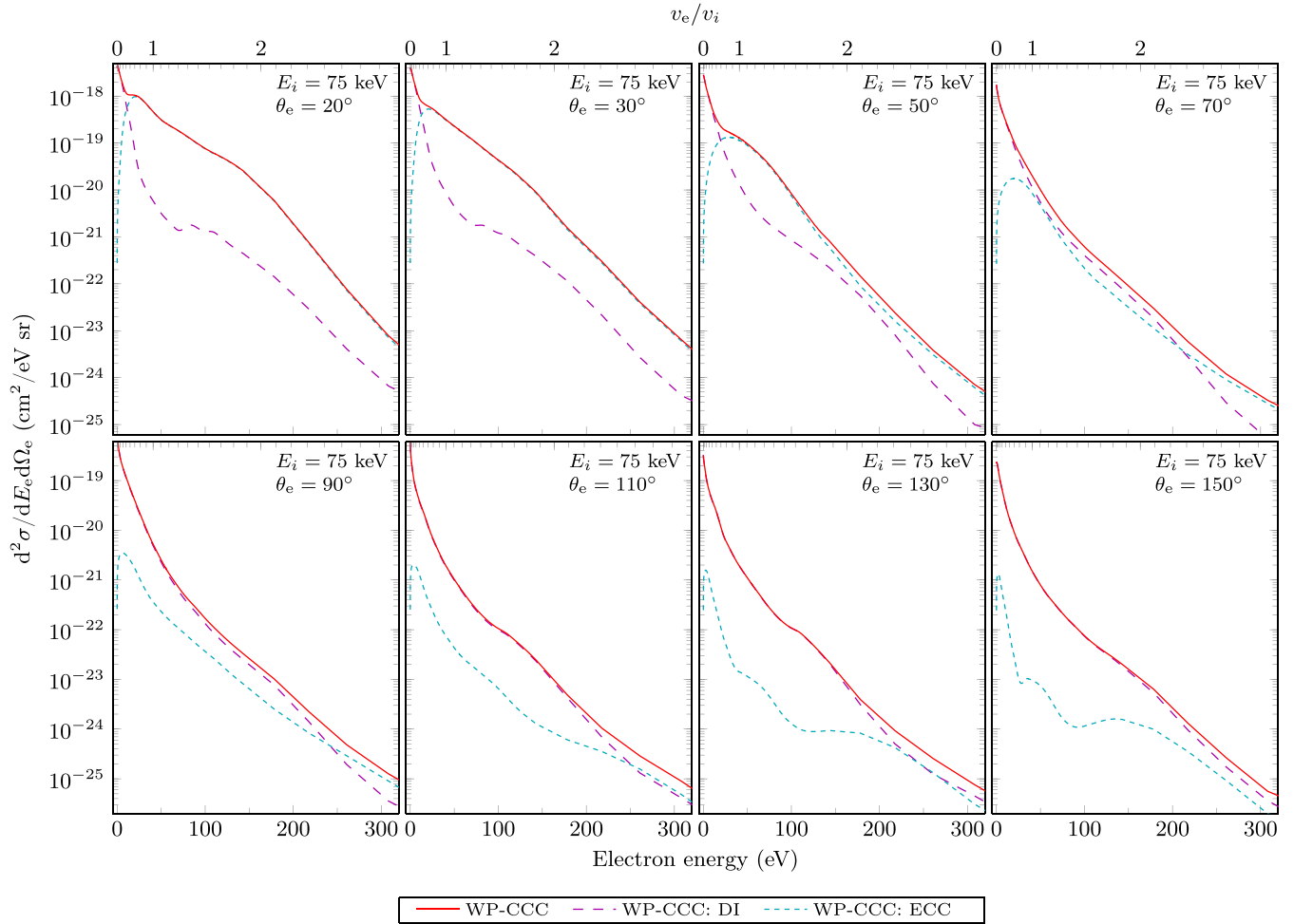


FIG. 4. Doubly differential cross sections for ionization in 75-keV  $p + \text{H}$  collisions as functions of the electron energy at various emission angles. The present WP-CCC results are shown along with the DI and ECC components.

In Figs. 2 and 3 we present results at 48 and 67 keV, respectively. Compared to the experimental data by Kerby III *et al.* [27], we generally find very good agreement across the entire range of electron energies and angles considered. The ECC peak is again visible at  $v_e = 0.7v_i$  in the WP-CCC results for  $20^\circ$  emission but has shifted to these energies. As the collision energy is increased, we also start seeing evidence of the binary-encounter mechanism as a slight hump near  $v_e = 2v_i$  in both experiment and theory. At these larger collision energies the CDW-EIS calculations by Kerby III *et al.* [27] show significant improvement in comparison to 20 keV. Still some underestimation of the most significant part of the cross section, the forward peak, is observed. Here, the CTMC method is also more accurate than at lower energies. However, when the emission angles are small the CTMC results are too large and for larger angles they fall off too slowly to be able to describe the experimental data. For  $110^\circ$ , a slight bump is seen in the present calculations at 70 eV. The experimental data fall off smoothly and are otherwise closely followed by the WP-CCC approach. A similar situation is observed at  $130^\circ$  where we can also see that the theories applied by Kerby III *et al.* [27] do not exhibit such behavior. Here the WP-CCC and CDW-EIS methods both agree with the measurements for small electron energies. For emission into  $150^\circ$ , our results

agree well with the experiment, although they fall off less steeply at energies above 30 eV. The WP-CCC results are the only calculations that consistently describe the experimental data at these large emission angles, although we observe a slight overestimation of the cross section when energetic electrons are emitted. This behavior was also observed for proton collisions with molecular hydrogen [51], where it was suggested the discrepancy may be the result of large experimental uncertainties or difficulties detecting the few electrons emitted in this region due to the relatively small cross section. Another possible explanation is that, in the present approach to calculating the total ionization amplitude, it is assumed that the electron experiences a weaker effective charge at asymptotic distances than it might actually be in the physical system. That is, when the electron is ejected into large angles it should (in the physical system) see the two separate positive charges of the target and projectile nuclei. In our approach this particular asymptotic state of three unbound particles may not be modeled well. We note, however, that the discrepancy between the present results and the measurements by Kerby III *et al.* [27] for emission of fast electrons into backward directions is smaller than we observed for the  $p + \text{H}_2$  collision system in Refs. [50,51]. While approximations were used in those works to construct the  $\text{H}_2$  pseudostates, here we use the exact form

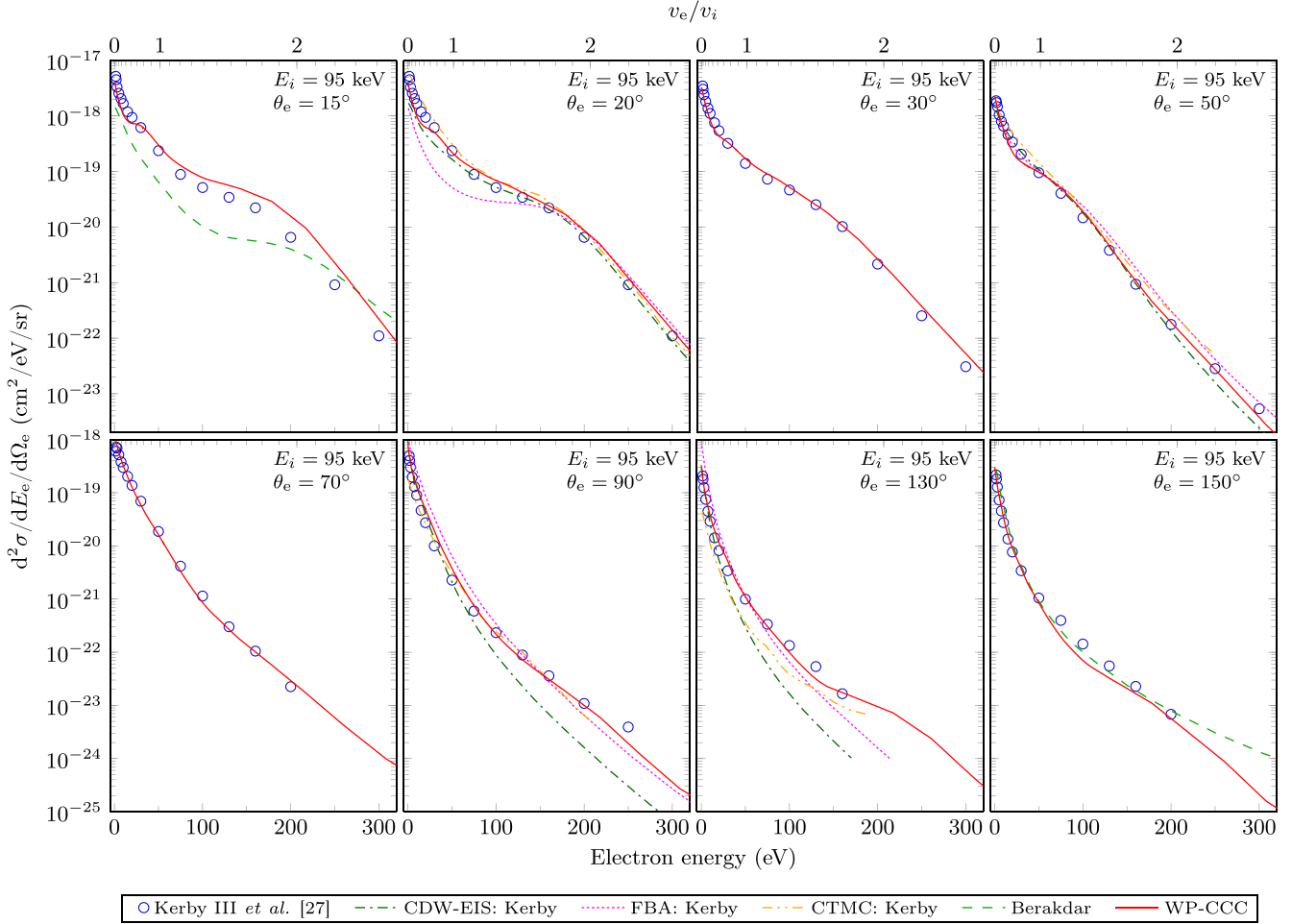


FIG. 5. Doubly differential cross sections for ionization in 95-keV  $p + \text{H}$  collisions as functions of the electron energy at various emission angles. Experimental data are by Kerby III *et al.* [27]. Theoretical results are the present WP-CCC approach, FBA, CDW-EIS approach, and CTMC approach by Kerby III *et al.* [27] and the three-body Coulomb method by Berakdar [37].

of the potential to create the hydrogen atom structure. The improved accuracy in describing the target herein may also contribute to the observed agreement with the experimental results.

In Fig. 4 we present results at a collision energy of 75 keV. This is an important energy near the maximum of the TICS and has received considerable attention at the fully differential level for various collision species [5,8,38]. Although there are no measurements or other theoretical calculations available at 75 keV for the presently considered cross section in  $p + \text{H}$  collisions, we present results at this energy together with the separate DI and ECC contributions. This allows us to analyze the significance of each mechanism in the different kinematic regions considered in this paper. We note that the relative contribution of each ionization channel is somewhat similar for all collision energies considered in this paper. Therefore, we show them only at 75 keV to prevent crowding of the other figures. The upper-left panel in Fig. 4 reveals that the small dip seen in the WP-CCC result near  $v_e = 0.5v_i$  occurs where the DI and ECC contribute equally. At smaller energies the cross section is dominated by the DI, whereas at larger energies it is dominated by ECC. We can also see the ECC peak. In the forward direction it occurs at  $v_e = v_i$ ,

but at  $20^\circ$  our results demonstrate that it has shifted towards smaller energies. Moving across the first row of Fig. 4, we observe that as the emission angle increases to  $70^\circ$  DI becomes more important. Meanwhile, the ECC mechanism gradually becomes less important as the emission angle increases. At  $70^\circ$ , DI still dominates for small energies, but when  $v_e > v_i$  both mechanisms are equally important. For emission at  $90^\circ$ , the cross section is dominated by DI up until 200 eV, after which both ionization mechanisms contribute equally to the total result. In the final three panels we see that DI is the most important process when electrons are emitted into the backward direction. Only for very fast electrons does the ECC mechanism contribute for emission angles greater than  $90^\circ$ . Physically this makes sense as one expects electrons emitted at these angles to be mainly influenced by the target ion.

Figure 5 shows our results for 95-keV collisions in comparison with the experimental data and theoretical results by Kerby III *et al.* [27] as well as the first-order perturbative calculations by Berakdar [37] available only at  $15^\circ$  and  $150^\circ$ . For emission into  $15^\circ$  our results accurately describe the forward peak at very small energies and show a slight bump near the expected position of the ECC peak, while the calculations by Berakdar [37] fail to display this fundamental feature.



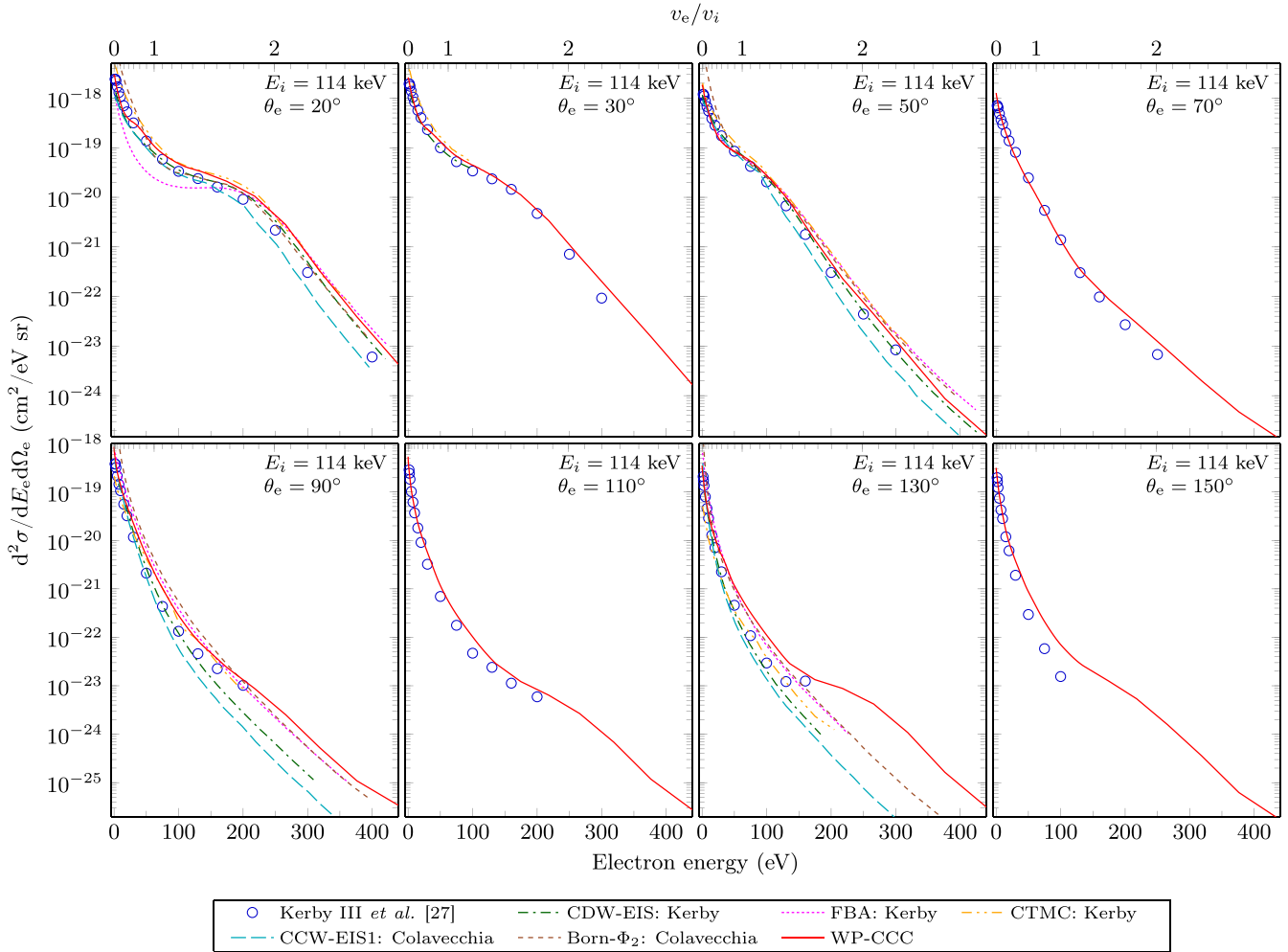


FIG. 6. Doubly differential cross sections for ionization in 114-keV  $p + \text{H}$  collisions as functions of the electron energy at various emission angles. Experimental data are by Kerby III *et al.* [27]. Theoretical results are the present WP-CCC approach, FBA, CDW-EIS approach, and CTMC approach by Kerby III *et al.* [27] and the CCW-EIS1 and Born- $\Phi_2$  methods by Colavecchia *et al.* [36].

The WP-CCC calculations slightly overestimate the binary-encounter peak, a result also observed in previous applications of the WP-CCC approach to  $p + \text{H}_2$  [51] and  $p + \text{He}$  [47] collisions. The calculations by Berakdar [37] significantly differ from the experimental data, underestimating the cross section below 200 eV and overestimating it above this energy. At the other angles for which experimental data are available, we observe a similar situation as for lower collision energies. Specifically, for the smaller emission angles, we find that the CDW-EIS calculations underestimate the measurements and the CTMC results overestimate them, especially for slow electrons. The WP-CCC results are the only calculations that consistently describe the experimental data. For ejection into the backwards direction the perturbative methods fall off too steeply and the CTMC results are overall too small. Meanwhile the present calculations follow the measurements closely even at  $150^\circ$ . Somewhat unexpectedly, so do the calculations by Berakdar [37], despite failing to describe the experiment for smaller angles, which can be considered a less stringent test for the theory.

The largest collision energy considered in this paper is 114 keV. Our results are presented in Fig. 6 where we observe

excellent agreement with the measurements by Kerby III *et al.* [27]. The various theories applied by Kerby III *et al.* [27] exhibit a similar level of agreement with the data as at 95 keV. At 114 keV we are also able to compare our results to those obtained using the Born- $\Phi_2$  and CCW-EIS1 approaches by Colavecchia *et al.* [36]. We see that the Born- $\Phi_2$  method provides improvement over the FBA results from Kerby III *et al.* [27], although it overestimates the data for small energies. The CCW-EIS1 result is identical to the CDW-EIS one up until the matching speed; however, after this point, the former underestimates the experiment while the latter overestimates it.

## V. CONCLUSION

In conclusion, we have applied the two-center WP-CCC method to the calculation of the differential cross section for ionization in proton collisions with atomic hydrogen. Being the simplest ion-atom collisions in which electron-capture can occur,  $p + \text{H}$  scattering has provided a benchmark system for theory since the inception of quantum mechanics. Previously available calculations based on perturbative and classical methods sometimes agreed with the experimental

measurements but could not consistently describe the data. The present results demonstrate that close-coupling methods are capable of accurately modeling the energy and angular distribution of ejected electrons in intermediate-energy collisions. Furthermore, we have significantly extended the range of electron energies for which theoretical data are available. We have also provided results for many ejection angles. Another unique feature of our method is the ability to distinguish between the direct ionization and electron capture into the continuum mechanisms. This allowed us to analyze their relative contributions to the total DDCS. While both mechanisms are found to be essential for accurately modeling the energy and angular distribution of emitted electrons, it is observed that in some kinematic regions one or the other process dominates: slow electrons are mainly the result of DI whereas fast electrons (especially in the forward direction) are the result of ECC.

Next we will apply the method to calculate the fully differential cross section for ionization. This represents the most detailed quantity and is very difficult to model. Currently, there is significant disagreement between the perturbative calculations and experimental data for the FDCS for ionization in  $p + \text{H}_2$  collisions. This discrepancy has been observed in studies by Schulz *et al.* [8] and Dhital *et al.* [5]. It has been proposed that the observed discrepancies between theory and experiment are due to the strong effects of coupling at intermediate energies that are not accounted for in the presently available perturbative calculations. Having established the ro-

business of the WP-CCC approach to differential ionization by studying both singly [45,46,62] and doubly [47,48,50,52] differential cross sections for various collision systems, we can now confidently apply it to this problem. However, the currently available experimental data are for  $\text{H}_2$  and He. This is much more difficult to accurately model than the atomic target. Similar fully differential measurements for  $p + \text{H}$  collisions would provide a very solid foundation for studying the FDCS since they would admit very accurate calculations using well-established structure models for atomic hydrogen.

## ACKNOWLEDGMENTS

This work was supported by the Australian Research Council. We also acknowledge the resources and services of the Pawsey Supercomputing Centre and the National Computing Infrastructure. This work also used the Expanse supercomputer at SDSC through the Advanced Cyberinfrastructure Coordination Ecosystem: Services and Support program. N.W.A. acknowledges support through an Australian Government Research Training Program Scholarship. K.H.S. acknowledges the contribution of an Australian Government Research Training Program Scholarship, and the support of the Forrest Research Foundation. M.S.S. acknowledges support from the Deutsche Forschungsgemeinschaft and Bundesministerium für Bildung und Forschung. M.S. is grateful for the support from the National Science Foundation under Grant No. PHY-2011307.

- 
- [1] C. Hill, D. Dipti, K. Heinola, A. Dubois, N. Sisourat, A. Taoutioui, H. Agueny, K. Tókési, I. Ziaecian, C. Illescas *et al.*, *Nucl. Fusion* **63**, 125001 (2023).
  - [2] D. Belkić, *J. Math. Chem.* **47**, 1366 (2010).
  - [3] *Ion-Atom Collisions: The Few-Body Problem in Dynamic Systems*, edited by M. Schulz (De Gruyter, Berlin, 2019).
  - [4] *State-of-the-Art Reviews on Energetic Ion-Atom and Ion-Molecule Collisions*, edited by D. Belkić, I. Bray, and A. Kadyrov (World Scientific, Singapore, 2019).
  - [5] M. Dhital, S. Bastola, A. Silvus, J. Davis, B. R. Lamichhane, E. Ali, M. F. Ciappina, R. Lomsadze, A. Hasan, D. H. Madison, and M. Schulz, *Phys. Rev. A* **102**, 032818 (2020).
  - [6] L. P. H. Schmidt, M. S. Schöffler, T. Jahnke, H. Schmidt-Böcking, and R. Dörner, *Phys. Rev. A* **109**, 032811 (2024).
  - [7] J. Ullrich, R. Moshhammer, A. Dorn, R. Dörner, L. P. H. Schmidt, and H. Schmidt-Böcking, *Rep. Prog. Phys.* **66**, 1463 (2003).
  - [8] M. Schulz, A. Hasan, N. V. Maydanyuk, M. Foster, B. Tooke, and D. H. Madison, *Phys. Rev. A* **73**, 062704 (2006).
  - [9] A. Hasan, T. Arthanayaka, B. Lamichhane, S. Sharma, S. Gurung, J. Remolina, S. Akula, D. H. Madison, M. F. Ciappina, R. D. Rivarola *et al.*, *J. Phys. B* **49**, 04LT01 (2016).
  - [10] H. Gassert, O. Chuluunbaatar, M. Waitz, F. Trinter, H.-K. Kim, T. Bauer, A. Laucke, C. Müller, J. Voigtsberger, M. Weller *et al.*, *Phys. Rev. Lett.* **116**, 073201 (2016).
  - [11] J. R. Oppenheimer, *Phys. Rev.* **31**, 349 (1928).
  - [12] H. C. Brinkman and H. A. Kramers, *Proc. Natl. Acad. Sci. USA* **33**, 973 (1930).
  - [13] D. R. Bates and G. Griffing, *Proc. Phys. Soc. A* **66**, 961 (1953).
  - [14] J. D. Jackson and H. Schiff, *Phys. Rev.* **89**, 359 (1953).
  - [15] I. Cheshire, *Proc. Phys. Soc.* **84**, 89 (1964).
  - [16] D. Dewangan, *J. Phys. B* **8**, L119 (1975).
  - [17] D. Crothers and J. McCann, *J. Phys. B* **16**, 3229 (1983).
  - [18] R. D. Rivarola, O. A. Fojón, M. Ciappina, and D. Crothers, *Springer Handbook of Atomic, Molecular, and Optical Physics* (Springer, New York, 2023), pp. 813–828.
  - [19] D. R. Bates, *Proc. Phys. Soc.* **247**, 294 (1958).
  - [20] I. Cheshire, D. Gallaher, and A. J. Taylor, *J. Phys. B* **3**, 813 (1970).
  - [21] T. G. Winter and C. C. Lin, *Phys. Rev. A* **10**, 2141 (1974).
  - [22] D. Gallaher and L. Wilets, *Phys. Rev.* **169**, 139 (1968).
  - [23] R. Shakeshaft, *J. Phys. B* **8**, 1114 (1975).
  - [24] N. Toshima and J. Eichler, *Phys. Rev. Lett.* **66**, 1050 (1991).
  - [25] A. S. Kadyrov, I. B. Abdurakhmanov, I. Bray, and A. T. Stelbovics, *Phys. Rev. A* **80**, 022704 (2009).
  - [26] A. C. K. Leung and T. Kirchner, *Eur. Phys. J. D* **73**, 246 (2019).
  - [27] G. W. Kerby III, M. W. Gealy, Y.-Y. Hsu, M. E. Rudd, D. R. Schultz, and C. O. Reinhold, *Phys. Rev. A* **51**, 2256 (1995).
  - [28] G. W. McClure, *Phys. Rev.* **148**, 47 (1966).
  - [29] J. E. Bayfield, *Phys. Rev.* **182**, 115 (1969).
  - [30] A. B. Wittkower, G. Ryding, and H. B. Gilbody, *Proc. Phys. Soc.* **89**, 541 (1966).
  - [31] P. Hvelplund and A. Andersen, *Phys. Scr.* **26**, 375 (1982).
  - [32] M. B. Shah and H. B. Gilbody, *J. Phys. B* **14**, 2361 (1981).
  - [33] M. B. Shah, D. S. Elliot, and H. B. Gilbody, *J. Phys. B* **20**, 2481 (1987).

- [34] J. Macek, *Phys. Rev. A* **1**, 235 (1970).
- [35] L. H. Toburen and W. E. Wilson, *Phys. Rev. A* **5**, 247 (1972).
- [36] F. Colavecchia, G. Gasaneo, and C. Garibotti, *J. Phys. B* **33**, L467 (2000).
- [37] J. Berakdar, *Phys. Rev. Lett.* **78**, 2712 (1997).
- [38] S. Bastola, M. Dhital, B. Lamichhane, A. Silvus, R. Lomsadze, J. Davis, A. Hasan, A. Igarashi, and M. Schulz, *Phys. Rev. A* **105**, 032805 (2022).
- [39] S. Jones and D. H. Madison, *Phys. Rev. A* **65**, 052727 (2002).
- [40] U. Chowdhury, M. Schulz, and D. H. Madison, *Phys. Rev. A* **83**, 032712 (2011).
- [41] I. B. Abdurakhmanov, A. S. Kadyrov, and I. Bray, *Phys. Rev. A* **94**, 022703 (2016).
- [42] I. B. Abdurakhmanov, J. J. Bailey, A. S. Kadyrov, and I. Bray, *Phys. Rev. A* **97**, 032707 (2018).
- [43] A. S. Kadyrov, I. Bray, A. M. Mukhamedzhanov, and A. T. Stelbovics, *Ann. Phys. (NY)* **324**, 1516 (2009).
- [44] I. B. Abdurakhmanov, N. W. Antonio, M. Cytowski, and A. S. Kadyrov, [arXiv:2403.04252](https://arxiv.org/abs/2403.04252).
- [45] C. T. Plowman, K. H. Spicer, I. B. Abdurakhmanov, A. S. Kadyrov, and I. Bray, *Phys. Rev. A* **102**, 052810 (2020).
- [46] K. H. Spicer, C. T. Plowman, I. B. Abdurakhmanov, S. U. Alladustov, I. Bray, and A. S. Kadyrov, *Phys. Rev. A* **104**, 052815 (2021).
- [47] K. H. Spicer, C. T. Plowman, S. U. Alladustov, I. B. Abdurakhmanov, I. Bray, and A. S. Kadyrov, *Eur. Phys. J. D* **77**, 131 (2023).
- [48] K. H. Spicer, C. T. Plowman, M. Schulz, and A. S. Kadyrov, *Phys. Rev. A* **108**, 022803 (2023).
- [49] C. T. Plowman, I. B. Abdurakhmanov, I. Bray, and A. S. Kadyrov, *Eur. Phys. J. D* **76**, 129 (2022).
- [50] C. T. Plowman, I. B. Abdurakhmanov, I. Bray, and A. S. Kadyrov, *Phys. Rev. A* **107**, 032824 (2023).
- [51] C. T. Plowman, K. H. Spicer, and A. S. Kadyrov, *Atoms* **11**, 112 (2023).
- [52] C. T. Plowman, K. H. Spicer, M. Schulz, and A. S. Kadyrov, *Phys. Rev. A* **108**, 052809 (2023).
- [53] S. U. Alladustov, C. T. Plowman, I. B. Abdurakhmanov, I. Bray, and A. S. Kadyrov, *Phys. Rev. A* **106**, 062819 (2022).
- [54] S. U. Alladustov, C. T. Plowman, M. S. Schöffler, I. Bray, and A. S. Kadyrov, *Phys. Rev. A* **109**, 022805 (2024).
- [55] B. H. Bransden and M. R. C. McDowell, *Charge Exchange and the Theory of Ion-Atom Collisions* (Clarendon, Oxford, 1992).
- [56] A. S. Kadyrov, I. Bray, A. M. Mukhamedzhanov, and A. T. Stelbovics, *Phys. Rev. Lett.* **101**, 230405 (2008).
- [57] C. T. Plowman, Wave-packet convergent close-coupling approach to ion collisions with atoms and molecules, Ph.D. thesis, Curtin University, 2024.
- [58] I. B. Abdurakhmanov, C. T. Plowman, A. S. Kadyrov, I. Bray, and A. M. Mukhamedzhanov, *J. Phys. B* **53**, 145201 (2020).
- [59] K. H. Spicer, C. T. Plowman, N. W. Antonio, M. S. Schöffler, M. Schulz, and A. S. Kadyrov, *Phys. Rev. A* **109**, 062805 (2024).
- [60] C. Illescas, B. Pons, and A. Riera, *Phys. Rev. A* **65**, 030703 (2002).
- [61] M. B. Shah, C. McGrath, B. Pons, A. Riera, H. Luna, D. S. F. Crothers, S. F. C. O'Rourke, and H. B. Gilbody, *Phys. Rev. A* **67**, 010704 (2003).
- [62] C. T. Plowman, I. B. Abdurakhmanov, I. Bray, and A. S. Kadyrov, *Eur. Phys. J. D* **76**, 31 (2022).